IEEE Access
Multidisciplinary | Rapid Review | Open Access Journal

Received May 21, 2019, accepted June 10, 2019, date of publication June 17, 2019, date of current version July 3, 2019.

Digital Object Identifier 10.1109/ACCESS.2019.2923313

LPV-Based Self-Adaption Integral Sliding Mode Controller With L_2 Gain Performance for a Morphing Aircraft

QIAN WU, ZHENGHUA LIU, FANNING LIU, AND XUEKUN CHEN
School of Automation Science and Electrical Engineering, Beihang University, Beijing 100083, China
Corresponding authors: Qian Wu (wqhrdyx@126.com) and Zhenghua Liu (lzh@buaa.edu.cn)

This work was supported by the Aeronautical Science Foundation of China under Grant 20175751028.

ABSTRACT This paper designs a parameter-dependent self-adaption integral sliding mode controller which converges the system in a finite time while focusing on an uncertain linear parameter varying (LPV) model of a variant aircraft that has a large-scale variation of the sweep angle and an extension. This design promotes the robustness and L_2 performance of the aircraft's speed and altitude during the variant process. According to the longitudinal nonlinear model of a morphing aircraft obtained by the KANE method, the LPV model with the stretch and the sweep angle as the time-varying parameters is derived, and then, the equivalent linear time-invariant (LTI) system is obtained by the linear fractional representation (LFR). Furthermore, the state feedback LFR-H_∞ controller has deduced from the linear matrix inequality (LMI) constraints, and then, the existing conditions of the integral sliding mode are obtained from the pole assignment. There are significant uncertainties and disturbances when the linear controller acts on the nonlinear system. Therefore, an adaptive algorithm is introduced to further improve the robustness of the integral sliding mode controller. Moreover, a parameter-dependent Lyapunov function analysis shows that the designed adaptive integral sliding mode control rate can converge the LPV system trajectories to the integral sliding mode surface in a finite time. The comparative simulation results of the nonlinear model of the morphing aircraft indicate the robustness and effectiveness of this approach. The method designed in this paper can be extended to general LPV systems.

INDEX TERMS Morphing Aircraft, robust control, LPV, integral sliding mode, adaptive control.

I. INTRODUCTION

A morphing aircraft is an advanced aircraft that enables the use of a single aircraft for multitasking capabilities, which achieves different aerodynamic characteristics by changing the shape of the structure during flight, promoting optimal aerodynamic flight under the full range of envelopes. This type of aircraft not only solves the aerodynamic shape of the rationally optimized configuration in the early stage but also can be compared with the later multitask execution [1]–[3]. Hence, morphing is a promising enabling technology for next-generation aircraft [4]. However, the deformation freedom of the variant aircraft brings complex changes to its configuration parameters and aerodynamic parameters, such as the exhibition length, chord length, centroid, and moment of inertia. Therefore, the flight control system of the morphing aircraft inevitably undertakes an arduous guarantee mission. For more than a century, the morphing aircraft has undergone a leap-forward development from simple implementation to the combination of intelligent materials and advanced control methods and has achieved fruitful research results.

The accurate establishment and reasonable form transformation of the variant aircraft dynamics model play an important role in the controller design. In the research of dynamic modeling of variant aircraft, some researchers have used the conventional single rigid body modeling method [5], which considers only the change of aerodynamic parameters with the morphing process, ignoring the changes such as the mass distribution and position of the centroid. Therefore, because of the multiple variant structures, the single rigid body modeling method is unable to accurately describe the dynamic

The associate editor coordinating the review of this manuscript and approving it for publication was Jun Hu.

characteristics of the variant aircraft. Hence, the nonlinear model of the variant aircraft obtained by the multibody modeling method can better reflect its real dynamic characteristics. A flight mechanics modeling method is proposed to solve the time-varying characteristics of the aerodynamic parameters, moment of inertia and centroid of a variant aircraft during the variant process, and flight simulation verification is carried out with the ''gull wing'' aircraft [6]. The Kane multibody modeling method is used to establish a nonlinear dynamic model including the variant structure of the morphing aircraft [7], [8].

The design of a flight control system is an important research direction because of its complex characteristics and uncertainty during the variant process. At present, the method of controller design is mainly divided into two directions: the nonlinear controller and the linear controller. From the aspects of algorithm maturity and design experience, it is very difficult to directly design a controller for complex nonlinear systems. However, there are still many studies on controller design for nonlinear models of morphing aircraft. In [9]–[11], the continuous change of sweep angle is regarded as the controller input quantity; furthermore, the adaptive evaluation network structure and the nonlinear dynamic inverse decoupling method are used to realize the optimized tracking controller design of the variant aircraft. With the assistance of morphing capability, the maneuverability of the aircraft has been significantly improved. For aircraft capable of large-scale deformation, the attitude stabilization and trajectory tracking controller for longitudinal motion is designed by calculating the relationship between its dynamic characteristics and the rate of change for the wing sweep angle [12], [13]. Based on the uncertainty of the morphing aircraft model and the input-output boundary constraints, an adaptive neuron dynamic surface controller is designed by the barrier Lyapunov function. Reference [14] computationally solves the aerodynamic parameters of the morphing aircraft and obtains its nonlinear model of it the morphing aircraft and obtains its nonlinear model. The adaptive control system with the inner ring providing deformation control and the outer ring providing flight control is designed. Linear controller design methods are more mature and less complex than nonlinear controller design methods. Therefore, how to ensure that the established mathematical model conforms to the dynamic characteristics of the variant aircraft and that the robust controller designed on this basis can ensure the smoothness of the dynamic output of the variant process has become the focus of research on morphing aircraft. Linear controller designs for morphing aircraft are mostly based on the LPV model because this model can include deformation parameters and characteristics of the operating point over time. To date, there has been a substantial amount of research on the design of morphing aircraft controllers based on the LPV model. In [15], a gain scheduling controller with LMI conditions is designed for the LPV model of a type of spanned morphing aircraft. Based on the speed linearization, the LPV model of the variant aircraft is established, and a robust H_∞ feedback controller is designed in [16]. A two-layer closed-loop system with feedback from the self-tuning controller is constructed for the LPV model of a folding wing aircraft [17], [18]. However, to adopt the multibody LPV model theorem to make the late H_∞ controller design eliminate infinite constraints, the coefficient matrix of the LPV model must be constructed as an affine parameter-dependent form. Therefore, it is impossible to accurately express the dynamic characteristics of a morphing aircraft in which a plurality of deformation parameters exist. At the same time, the above literature does not consider the existence of model perturbation and interference, and later studies have shown that the H_∞-type controller has a poor control effect under this condition [7].

The development of sliding mode controllers has brought new ideas to solve the controller design of uncertain LPV systems since the sliding surfaces are insensitive to matched or mismatched uncertainties [19]. To improve the resistance of the controller to the perturbation and interference of the LPV model, the sliding mode controller is designed by the LMI based on the description of the LTI system to improve the robustness of the system [20]–[22]. Among those references, [21] guarantees the L_2 performance of the system, and [22] introduces an adaptive control algorithm. However, all of those solutions are restricted to the single operational condition, and most of them are sliding mode observers for special LPV applications only [23], [24]. To further improve the problems in the above documents, a class of parameter-dependent sliding mode controllers with finite time convergence is derived using LMI conditions, which guarantees the stability of a complex variant aircraft morphing process, and a detailed theoretical derivation is carried out in [7]. However, the single selection of its Lyapunov matrix leads to the sliding surface not achieving a true parametric dependence. Furthermore, in the absence of model parameter perturbation and interference, the quality of this sliding mode controller is lower than that of the H_∞ controller with reasonable parameter selection. It can be seen from the above review that research on the design of sliding mode controllers for common LPV systems is limited. Based on the above literature, the advantages of the integral sliding mode controller have attracted our attention. The introduction of the integral term not only changes the sliding surface with the change of time-varying parameters but also realizes the theoretical parameter-dependent form of the sliding surface and makes the output error converge to zero more efficiently.

Inspired by the above research, the robust integral sliding mode control problem for uncertain LPV systems of a type of large-scale morphing aircraft is studied in this paper. First, the nonlinear model based on the KANE multibody model is transformed to the uncertain LPV model. The convex multibody LPV model is further obtained, and then the LTI system form is derived. The above mathematical model serves as the basis for the controller design. Second, the existence conditions of the integral sliding surface that can converge the LPV system for a limited time are derived. Based on the

LMI existence condition, the LFR-H_∞ controller, which can guarantee the stability of the variant process, is designed, and the integral sliding mode controller, which makes the system have the same closed-loop pole, is derived by the pole configuration method. Then, in order to further suppress model perturbation and interference and improve the robustness of the system, the adaptive rate is introduced into the control law. Finally, the Lyapunov function proves that the parameter-dependent robust adaptive integral sliding mode controller can make the system trajectory converge to the sliding surface in a finite time to ensure the stability of the system.

The exact contributions of this paper over previous works are as follows:

- *The linearized LPV model of morphing aircraft has been extended to include a velocity integral term and a height integral term. The designed controller can not only maintain the height and speed of the system but also minimize the L_2 gain performance of the system.*
- *Unlike the cases of [15]–[18], the H_∞ controller design is carried out after converting the nonaffine LPV model of the morphing aircraft into the LFR form. Surpassing the limitations of the LPV model in the past literature requires the use of the affine form.*
- *Compared with the newly studied sliding mode controller [7], the adaptive integral sliding mode controller designed in this paper realizes the parameter-dependent form in the theoretical sense - the introduction of the integral term causes the sliding surface to change with the change of the deformation parameters. In addition, all the closed-loop poles can be arbitrarily placed, not just those for the reduced system in the sliding mode as in the prevailing literature. Hence, compared with that of the sliding mode controller designed in [7], the control quality is further improved, and the anti-interference ability and robustness of the system are improved compared with those of the LFR-H_∞ controller.*

The sections in this article are organized as follows. Useful preliminaries are given in Section II. Section III contains the establishment and transformation of the dynamic model of a morphing aircraft. Section IV deduces the existence conditions of the integral sliding surface based on the LFR-H_∞ controller. Then, we carry out the Lyapunov stability analysis. In Section V, numerical simulations are implemented to evaluate the performance of the adaptive integral sliding mode controller. The conclusion is shown in Section VI.

II. PRELIMINARY RESULTS

Lemma 1 (Vertex Properties of Cellular LPV Systems [25]): If the LPV system matrix can be described as a convex combination of vertex matrices (polymorphic structure)

$$Co\{A_i, i = 1, 2, \ldots, k\} := \left\{ \sum_{i=1}^{k} \alpha_i A_i | \alpha_i \geq 0, \sum_{i=1}^{k} \alpha_i = 1 \right\}, \tag{1}$$

then the combination of controllers designed at the vertex can be applied to the whole LPV system.

Lemma 2 (Boundary Reality Theorem [26], [27]): Consider the system (2)

$$\begin{cases} \dot{x} = Ax + Bw \\ z = Cx + Dw \end{cases}, \tag{2}$$

where x, w, and z are the system states, inputs, and outputs, respectively. Let the constant $\gamma > 0$; then, the system is progressively stable, and the transfer function from w to z satisfies $\|T_{zw}(s)\|_\infty < \gamma$ if and only if there is a positive definite symmetric matrix $P > 0$, establishing (3).

$$\begin{bmatrix} A^T P + PA & PB & C^T \\ B^T P & -\gamma I & D^T \\ C & D & -\gamma I \end{bmatrix} < 0. \tag{3}$$

Lemma 3 (Quadratic L_2 Gain Characterization [28]): Consider the LFR system given in (4)

$$\begin{cases} \dot{x} = Ax + B_q q + B_w w \\ p = C_p x + D_{pq} n + D_{pw} w \\ z = C_z x + D_{zq} q + D_{zw} w \\ q = \Delta(\theta) p \\ \Delta(\theta) = diag(\theta_1 I_{s1}, \ldots, \theta_m I_{sm}). \end{cases} \tag{4}$$

If there exist matrices $P \in S_+^n$ and $\Pi \in R^{n_p \times m_p}$ and a real scalar $\gamma > 0$ such that

$$\Omega_{P,i} + U_{P,i}^T \Pi V_P + W_P^T \Pi V_{P,i} < 0, \quad i = 1, \ldots, r, \tag{5}$$

where

$$\begin{aligned} \Omega_{P,i} &= \begin{bmatrix} A^T P + PA & PB_{q,i} & PB_w & C_z^T \\ (PB_{q,i})^T & 0 & 0 & D_{zq,i}^T \\ (PB_w)^T & 0 & -\gamma I & D_{zw}^T \\ C_z & D_{zq,i} & D_{zw} & -\gamma I \end{bmatrix} \\ U_{P,i} &= \begin{bmatrix} C_p & -I + D_{pq,i} & D_{pw} & 0 \end{bmatrix} \\ V_P &= \begin{bmatrix} I & 0 \end{bmatrix}. \end{aligned} \tag{6}$$

then system (4) is quadratically stable, and the quadratic L_2 gain from w to z is less than or equal to γ for all values of the parameter θ.

Lemma 4 (Schur Complement Lemma [27]): For a given symmetric matrix

$$S = \begin{bmatrix} S_{11} & S_{12} \\ S_{21} & S_{22} \end{bmatrix}, \tag{7}$$

the following three conditions are equivalent

$$\begin{cases} S < 0 \\ S_{11} < 0, \quad S_{22} - S_{12}^T S_{11}^{-1} S_{12} < 0 \\ S_{22} < 0, \quad S_{11} - S_{12}^T S_{22}^{-1} S_{12} < 0. \end{cases} \tag{8}$$

Lemma 5 (Controllability Criterion): If the controllable matrix S_c of the linear stationary system (A, B) is defined as (9), the necessary and sufficient condition for the system to be fully controllable is (10).

$$S_c = \begin{bmatrix} B & AB & A^2 B & \ldots & A^{n-1} B \end{bmatrix}, \tag{9}$$

$$rank S_c = n. \tag{10}$$

III. MODELING AND SYSTEM DESCRIPTION

In this paper, a morphing aircraft with a variable wing length and sweep angle is chosen as the research object. The BQM-34 "Firebee" UAV produced by Teledyne-Ryan Company in the United States was used as the basic platform of the morphing aircraft design. The Firebee UAV is one of the most widely used drones and has the advantages of recyclable use, excellent performance and strong renovability. The three views of Firebee are shown in Fig. 1, and part of the basic configuration parameters are listed in Table 1. Other parameters can be referred to as described in [29].

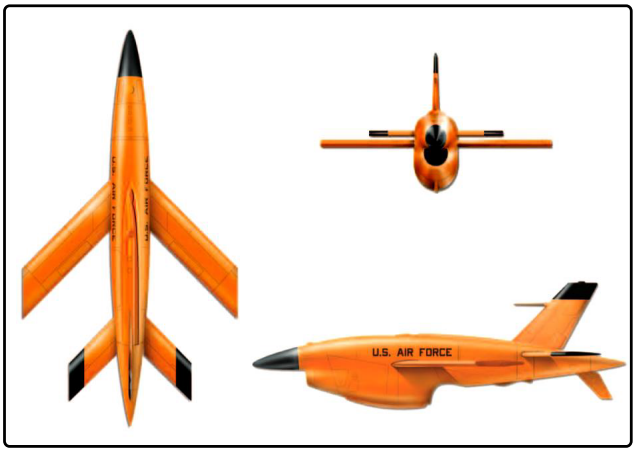

FIGURE 1. Three views of the Firebee UAV.

TABLE 1. Basic configuration parameters of the Firebee UAV.

Parameter/Unit	Basic Configuration
Length (m)	6.9
Span Length (m)	3.9
Height (m)	2.1
Weight (kg)	907
Maximum Flight Speed $(Mach)$	0.97
Lift limit (km)	18.3
Engine mounting angle $(^\circ)$	0

This paper replaces the wings with deformable wings that have variable sweep lengths and sweep angles. The wing swept angle can be changed in the range of $0^\circ - 45^\circ$ smoothly, and the complete wingspan can be varied from $5\ m - 9\ m$. Assume that the variant process is performed symmetrically and simultaneously on the left and right wings. Several typical appearances are shown in Fig. 2. For example, shape A has a large wingspan and no sweep angle, which increases the lift of the aircraft. Hence, this shape is suitable for the takeoff mission. Shape D is the high-speed profile with fully retracted wings and the maximum sweep angle.

This part is based on the longitudinal nonlinear model of the morphing aircraft obtained by Kane modeling. First, linearization is used to build the LPV model and then obtain the equivalent LTI model through LFR modeling. In this paper,

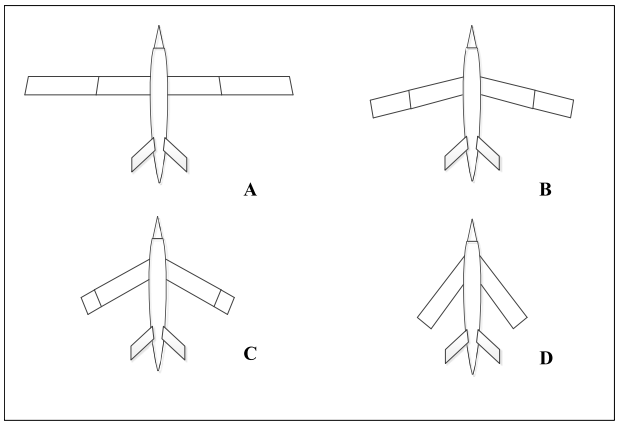

FIGURE 2. Some typical appearances of the morphing aircraft.

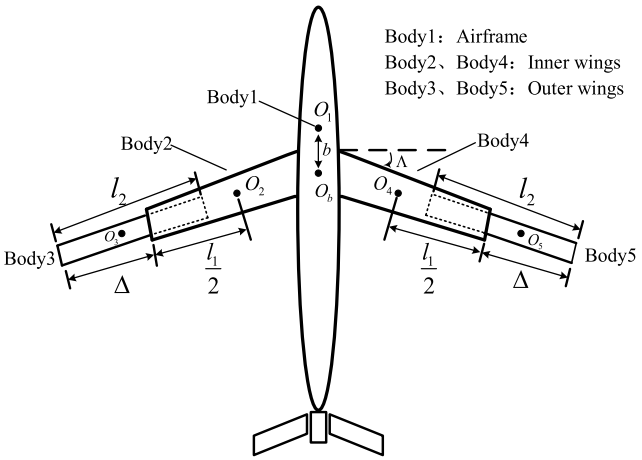

FIGURE 3. Depiction of the multibody representation.

TABLE 2. Variable values in the multibody model of the variant aircraft.

Parameter/Unit	Parameter values
$b\ (m)$	0.3
$\Lambda\ (^\circ)$	$0 - 45$
$\Delta\ (m)$	$0 - 2$
$l_1\ (m)$	2.5
$l_2\ (m)$	2.0

only the longitudinal movement of the aircraft is considered. The altitude is selected as $h_0 = 9144\ m$ and $V_0 = 0.5\ Mach$ ($V_0 \approx 170.15\ m/s$). Define the sweep angle and wingspan change rate $\lambda = \Lambda/45^\circ \in [0, 1]$ and $\xi = \Delta/l_1 \in [0, 0.8]$, respectively, where Λ is the sweep angle, Δ is the change quantity of the half wingspan and l_1 is the length of the inner wings. The labels for each part of the morphing aircraft are shown in Fig. 3. Table 2 lists the values of the variables shown in Fig. 3.

A. NONLINEAR MODEL FOR THE MORPHING AIRCRAFT

The dynamic model of the morphing aircraft is the basis for the control system design. Changes in the shape of the

aircraft lead to changes in the mass distribution, moment of inertia, etc. The conventional aircraft model is modeled as a single rigid body that cannot obtain an accurate mathematical model. Therefore, the multibody model based on the KANE modeling method is used for the nonlinear model of the morphing aircraft. The morphing aircraft nonlinear model is as follows [7], [8]

$$E\begin{bmatrix}\dot{V}\\ \dot{\alpha}\\ \dot{q}\\ \dot{\theta}\\ \dot{h}\end{bmatrix}=\begin{bmatrix}F_1\\ F_2\\ F_3\\ q\\ V\sin(\theta-\alpha)\end{bmatrix}+\begin{bmatrix}W_1\\ W_2\\ W_3\\ 0\\ 0\end{bmatrix}, \tag{11}$$

where

$$E=\begin{bmatrix}m_t & 0 & \sin\alpha e & 0 & 0\\ 0 & m_tV & \cos\alpha e & 0 & 0\\ \sin\alpha e & V\cos\alpha e & E_{33} & 0 & 0\\ 0 & 0 & 0 & 1 & 0\\ 0 & 0 & 0 & 0 & 1\end{bmatrix}, \tag{12}$$

$$\begin{cases}F_1 = T\cos\alpha - D - m_tg\sin(\theta-\alpha)\\ \quad -q^2\cos\alpha(m_1l_1\sin\Lambda + 2m_2l_\Delta\sin\Lambda - m_bb)\\ F_2 = -\sin\alpha T - L + m_tg\cos(\theta-\alpha) + m_tqV\\ \quad +q^2\sin\alpha(m_1l_1\sin\Lambda + 2m_2l_\Delta\sin\Lambda - m_bb)\\ F_3 = b\sin\alpha D + b\cos\alpha L + M_y + g\cos\theta\\ \quad (l_1m_1\sin\Lambda + 2l_\Delta m_2\sin\Lambda - m_bb)\\ \quad +qV\cos\alpha(l_1m_1\sin\Lambda + 2m_2l_\Delta\sin\Lambda - m_bb),\end{cases} \tag{13}$$

$$\begin{cases}W_1 = -m_1l_1\cos\alpha(\Lambda'^2\sin\Lambda - \Lambda''\cos\Lambda)\\ \quad -2m_2\cos\alpha(-3\Delta'\Lambda'\cos\Lambda - \Delta''\sin\Lambda\\ \quad +2l_\Delta\Lambda'^2\sin\Lambda\\ \quad -\Lambda''l_\Delta\cos\Lambda) - 2qm_1l_1\Lambda''\sin\alpha\cos\Lambda\\ \quad -m_2\sin\alpha(4q\Delta'\sin\Lambda + 4ql_\Delta\Lambda'\cos\Lambda)\\ W_2 = m_1l_1\sin\alpha(\Lambda'^2\sin\Lambda - \Lambda''\cos\Lambda) + 2m_2\sin\alpha\\ \quad (-3\Delta'\Lambda'\cos\Lambda - \Delta''\sin\Lambda + 2l_\Delta\Lambda'^2\sin\Lambda\\ \quad -\Lambda''l_\Delta\cos\Lambda) - 2qm_1l_1\Lambda'\cos\alpha\cos\Lambda\\ \quad -m_2\cos\alpha(4q\Delta'\sin\Lambda + 4ql_\Delta\Lambda'\cos\Lambda)\\ W_3 = -qm_1l_1^2\Lambda'\sin\Lambda\cos\Lambda\\ \quad -2m_2l_\Delta\sin\Lambda(2q\Delta'\sin\Lambda\\ \quad +2ql_\Delta\Lambda'\cos\Lambda) - 2q\Lambda'(J_2+J_3)\sin\Lambda\cos\Lambda\end{cases}. \tag{14}$$

In E,

$$\begin{cases}e = (l_1m_1\sin\Lambda + 2m_2l_\Delta\sin\Lambda - m_bb)\\ E_{33} = m_bb^2 + \sin^2\Lambda[\frac{1}{2}l_1^2m_1 + 2m_2l_\Delta^2 + 2(J_2+J_3)] + J_y.\end{cases} \tag{15}$$

Among these parameters, m_t, m_b, m_1,m_2 are the quality of the whole aircraft, Body1, inner wing, and outer wing, respectively. V and h indicate the speed and height of the flight, respectively, α represents the angle of attack, and θ and q represent the pitch angle and pitch angular rate, respectively. J_y is the body longitudinal moment of inertia, and J_2 and J_3 represent the inertia of Body2 and Body3, respectively. Other variables are shown in Fig. 3. This paper considers only the longitudinal motion of the aircraft.

In (11), T,L, and D are respectively the thrust, lift and resistance of the aircraft determined by (16)

$$\begin{cases}D = QS_wC_{D_\alpha}(\alpha)\\ L = QS_wC_L = QS_w(C_{L_{\alpha=0}} + C_{L_\alpha}\alpha + C_{L_{\delta e}}\delta_e)\\ M = QS_w\bar{c}C_M = QS_w\bar{c}(C_{M_{\alpha=0}} + C_{M_\alpha}\alpha + C_{M_{\delta e}}\delta_e)\\ T = T_{\delta_T}\delta_T.\end{cases} \tag{16}$$

where

$$\begin{cases}C_D(\alpha) = 0.0257 - 0.0069\xi - 0.0036\lambda\\ \quad +(0.0014 - 0.0002\xi - 0.0008\lambda)\alpha\\ C_{L_{\alpha=0}} = 0.1417 + 0.0642\xi + 0.0209\lambda - 0.0291\xi^2\\ \quad -0.0336\lambda\xi - 0.1527\lambda^2 + 0.0159\lambda\xi^2\\ \quad -0.0025\lambda^2\xi + 0.0565\lambda^3\\ C_{L_\alpha} = 0.0979 + 0.0051\xi - 0.0148\lambda\\ \quad +0.0342\lambda\xi - 0.0632\lambda^2\\ \quad -0.1548\lambda^2\xi - 0.1925\lambda^3 + 0.1164\lambda^3\xi\\ \quad +0.0992\lambda^4\\ C_{L_{\delta e}} = 0.0038 - 0.0027\xi + 0.0012\xi^2\\ C_{M_{\alpha=0}} = 0.0357 - 0.0912\xi - 0.1026\lambda + 0.0702\xi^2\\ \quad -0.2233\lambda\xi + 0.0674\lambda^2 - 0.0264\xi^3\\ \quad -0.0192\lambda\xi^2 + 0.1672\lambda^2\xi\\ C_{M_\alpha} = -0.0293 - 0.0024\xi - 0.0245\lambda + 0.0083\xi^2\\ \quad -0.0649\lambda\xi - 0.0758\lambda^2 - 0.0932\lambda\xi^2\\ \quad -0.1684\lambda^2\xi\\ \quad +0.2344\lambda^3 - 0.3587\lambda^2\xi^2 + 0.1852\lambda^3\xi\\ \quad -0.1849\lambda^4\\ \quad -0.3052\lambda^3\xi^2 + 0.0346\lambda^4\xi + 0.0401\lambda^5\\ C_{M_{\delta e}} = -0.0142 + 0.0083\xi + 0.0032\lambda\\ \quad -0.0028\xi^2 - 0.001\lambda\xi.\end{cases} \tag{17}$$

In (16), Q is the atmosphere dynamic pressure, $\bar{c}$ is the average aerodynamic chord length, S_w is the reference area of the wings, $T_{\delta_T} = 129.27N/\%$ is the throttle opening coefficient, and δ_e, δ_T represent the elevator declination and throttle opening, respectively. In addition, C_L, C_M,C_D are the lift coefficient, pitch moment coefficient and thrust coefficient, respectively, which are functions of λ and ξ. C_L, C_M,C_D are fitted by the data obtained from DATCOM [30], a useful software package that can provide aerodynamic coefficients based on aircraft profile parameters.

B. POLYTOPIC LPV MODEL FOR THE MORPHING AIRCRAFT

In this paper, the LPV model of the morphing aircraft is chosen as a mathematical model for the controller design.

The Jacobian linearization method is used to transform the nonlinear variable parameter model (11) into a small linear perturbation model (18)

$$\dot{x} = A(\lambda, \xi)x + B(\lambda, \xi)u, \tag{18}$$

where

$$\begin{cases} A(\lambda,\xi) = \begin{bmatrix} A_{11}(\lambda,\xi) & A_{12}(\lambda,\xi) & 0 & -g & 0 & 0 & 0 \\ 0 & A_{22}(\lambda,\xi) & 1 & 0 & 0 & 0 & 0 \\ 0 & A_{32}(\lambda,\xi) & 0 & 0 & 0 & 0 & 0 \\ 0 & 0 & 1 & 0 & 0 & 0 & 0 \\ 0 & -V_0 & 0 & V_0 & 0 & 0 & 0 \\ 1 & 0 & 0 & 0 & 0 & 0 & 0 \\ 0 & 0 & 0 & 0 & 1 & 0 & 0 \end{bmatrix} \\ B(\lambda,\xi) = \begin{bmatrix} B_{11}(\lambda,\xi) & 0.1425 \\ B_{21}(\lambda,\xi) & 0 \\ B_{31}(\lambda,\xi) & 0 \\ 0 & 0 \\ 0 & 0 \\ 0 & 0 \\ 0 & 0 \end{bmatrix}. \end{cases} \tag{19}$$

$A_{11}, A_{12}, A_{22}, A_{32}, B_{11}, B_{21}, B_{31}$ are function expressions governed by λ and ξ, whose specific expressions are described in [7]. In (18), $x = [\Delta V \quad \Delta\alpha \quad \Delta q \quad \Delta\theta \quad \Delta h \quad \int e_v dt \quad \int e_h dt]^T$ are state quantities; $u = [\delta_e \quad \delta_T]^T$ are the elevator deflection and throttle control volume; and e_v, e_h are the deviations of speed and height relative to the instruction values, respectively. It is proven that the response curves of the LPV model and nonlinear model essentially coincide with each other when the vehicle is in an open-loop state. Therefore, the LPV model can be used as the basis of the controller design [7].

Remark 1: To minimize the L_2 gain performance of the outputs, the state matrix is extended to include the terms $\left[\int e_v dt \quad \int e_h dt\right]^T$. $\int e_v dt$ and $\int e_h dt$ are the error integrals of the speed and altitude, respectively. Considering the uncertainties and other disturbances of the system matrix, the system model (18) is extended to the following forms (20)

$$\begin{cases} \dot{x} = (A(\lambda,\xi) + \Delta A)x + B_1(\lambda,\xi)u + B_2 w \\ y = Cx + D_1 u + D_2 w, \end{cases} \tag{20}$$

where

$$\begin{cases} C = \begin{bmatrix} 0 & 0 & 0 & 0 & 0 & 1 & 0 \\ 0 & 0 & 0 & 0 & 0 & 0 & 1 \end{bmatrix} \\ D_1 = 0_{2\times 2} \\ D_2 = 0_{2\times 1}. \end{cases} \tag{21}$$

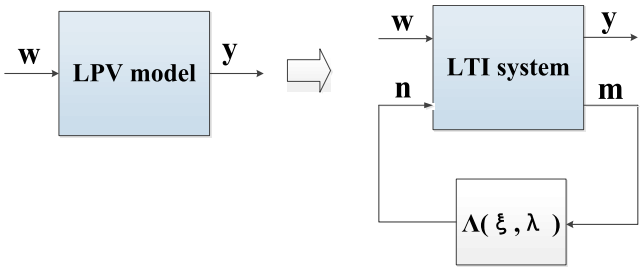

FIGURE 4. Equivalent graphs of the LPV and LFR systems.

To reduce the complexity of the controller design by directly applying Lemma 1 in the later work, the equivalent polytopic structure with k vertices of the LPV model (20) is obtained by the tensor product conversion method of high-order singular value decomposition (HOSVD). The specific decomposition process is described in [31], and the details are not discussed here. Then, we can obtain (22):

$$\begin{cases} \dot{x} = (Co\{A_i, i = 1, 2, \ldots, k\} + \Delta A)x \\ +Co\{B_{1i}, i = 1, 2, \ldots, k\}u + B_2 w \\ y = Cx + D_1 u + D_2 w \end{cases} \tag{22}$$

where

$$\begin{cases} Co\{A_i, i = 1, 2, \ldots, k\} \\ \quad = \left\{\sum_{i=1}^{k} \alpha_i A_i | \alpha_i \geq 0, \sum_{i=1}^{k} \alpha_i = 1\right\} \\ Co\{B_{1i}, i = 1, 2, \ldots, k\} \\ \quad = \left\{\sum_{i=1}^{k} \beta_i B_{1i} | \beta_i \geq 0, \sum_{i=1}^{k} \beta_i = 1\right\}. \end{cases} \tag{23}$$

C. LFR MODEL FOR THE MORPHING AIRCRAFT

$A(\lambda, \xi)$ is a nonaffine parameter-dependent form of λ,ξ, so the traditional polytopic design method cannot be used to design H_∞ controller [26]. This section uses the LFR method [28] to transform the LPV model (20) into the LTI model as the basis of the H_∞ controller design, as shown in Fig. 4. The transformation of the equation of state is in (24), as shown at the bottom of this page.

Therefore, the equivalent LFR form of (24) can be expressed as (25), which is the model basis of the H_∞ controller design.

$$\begin{cases} \dot{x} = \underline{A}x + B_n n + B_u u + B_w w \\ m = C_m x + D_{mn} n + D_{mu} u + D_{mw} w \\ y = C_y x + D_{yn} n + D_{yu} u + D_{yw} w \\ n = \Lambda(\lambda, \xi)m \\ \Lambda(\lambda, \xi) = diag(\lambda I_1, \xi I_2) \end{cases} \tag{25}$$

$$\begin{bmatrix} A(\lambda,\xi) & B_1(\lambda,\xi) & B_2 \\ C & D_1 & D_2 \end{bmatrix} = \begin{bmatrix} \underline{A} & B_u & B_w \\ C_y & D_{yw} & D_{yu} \end{bmatrix} + \begin{bmatrix} B_n \\ D_{yn} \end{bmatrix} \times \Lambda(\lambda,\xi)(I - D_{mn}\Lambda(\lambda,\xi))^{-1} \begin{bmatrix} C_m & D_{mu} & D_{mw} \end{bmatrix} \tag{24}$$

The specific definitions of the matrices in (25) are given in the Appendix. In this model, only $\Lambda(\lambda, \xi)$ is a matrix with variable parameters, and it can be transformed into a polytopic structure according to the vertex selected in Section II.B. Hence, $\Lambda(\lambda, \xi)$ can be expressed as $Co\{\Lambda_i, i = 1, 2, \ldots k\}$. At this point, the LTI form of this morphing aircraft is obtained, and the H_∞ controller can be designed based on the model.

IV. ADAPTIVE INTEGRAL SLIDING MODE CONTROLLER DESIGN

This section designs the adaptive integral sliding mode controller for the morphing aircraft. First, based on the feedback matrix of the LFR-H_∞ infinite controller of the variant aircraft, the conditions of the integral sliding mode surface are derived. Then, the adaptive integral sliding mode control law with the adaptive rate is derived according to the selected sliding surface. Finally, proof of Lyapunov stability is carried out.

A. CHOOSING THE INTEGRAL SLIDING MODE SURFACE BASED ON THE LFR-H_∞ STATE FEEDBACK

In the past, it has been found that the H_∞ controller can achieve better control performance than the existing sliding mode controller when the feedback matrix is adjusted suitably. However, in the case of parameter perturbation, the stability of the sliding mode controller is much better than that of the H_∞ controller, whose control effect is obviously reduced. In this part, the feedback matrix of the LFR-H_∞ controller is designed first. Then, the integral sliding surface with the same control function is derived [32].

Theorem 1: Define the integral sliding surface as follows

$$s = -E(\lambda, \xi)x + F\int_0^t ed\tau, \tag{26}$$

where the matrix $E(\lambda, \xi) \in R^{2\times 7}$ ensures that $(E(\lambda, \xi)B(\lambda, \xi))$ is a nonsingular matrix; $F \in R^{2\times 2}$ is a full rank weighting matrix; and $e \in R^{2\times 2}$ is the difference between the actual output y and the given output $\bar{y}$.

Considering the polytopic LPV model (22), evaluate the scalar $\gamma > 0$. If the LFR model (25) of the same system satisfies the LMI condition (27) and the integral sliding surface is selected by condition (29), as shown at the bottom of this page, then the integral sliding surface (26) exists, and the system has robust stability with L_2 gain performance. Furthermore, the closed-loop poles of the integral sliding mode are exactly the eigenvalues of the desired system with the LFR-H_∞ controller.

$$\Omega_{Q,i} + U_{Q,i}^T M W_{Q,i} + W_{Q,i}^T M U_{Q,i} < 0. \tag{27}$$

For the specific form of $U_{Q,i}$, $\Omega_{Q,i}$ and $W_{Q,i}$, see (28), as shown at the bottom of this page. In (29), $Co\{K_i, i = 1, 2, \ldots, k\}$ are the polytopic forms of $K(\lambda, \xi)$ solved from (28) by $K_i = (KQ)_i/Q$, $Q = Q^T > 0$ and $M = M^T$.

Proof: First, it is proven that the pair $(A(\xi, \lambda), B_1(\xi, \lambda))$ is completely controllable over the entire variable trajectory $\lambda \in [0, 1]$ and $\xi \in [0, 0.8]$.

For the polytopic LPV model (22) of the morphing aircraft, the calculation verification (30) is established:

$$\begin{aligned} rankS_{c1} &= rank\begin{bmatrix} B_{11} & A_1B_{11} & \ldots & A_1^6B_{11}\end{bmatrix} = 7\\ rankS_{c2} &= rank\begin{bmatrix} B_{12} & A_2B_{12} & \ldots & A_2^6B_{12}\end{bmatrix} = 7\\ &\ldots\\ rankS_{c2} &= rank\begin{bmatrix} B_{1k} & A_kB_{1k} & \ldots & A_k^6B_{1k}\end{bmatrix} = 7 \end{aligned} \tag{30}$$

As specified by Lemma 5, the LPV system (20) is completely controllable at the vertices. Because of Lemma 1, the completely controllable nature of the vertices can be extended to the entire LPV system (20) with $\lambda \in [0, 1]$ and $\xi \in [0, 0.8]$.

Second, design the H_∞ controller based on the LFR model to construct a closed-loop system of the LPV model for the morphing aircraft.

Consider the following form of the LPV model

$$\begin{cases} \dot{x} = A(\lambda,\xi)x + B_2w \\ y = Cx + D_2w, \end{cases} \tag{31}$$

According to Lemma 2, if and only if there is a real matrix $P = P^T > 0$ that satisfies the LMI constraint (32) is the system quadratically stable with an induced L_2 gain of less than γ.

$$\begin{bmatrix} PA(\lambda,\xi) + A^T(\lambda,\xi)P & PB_2(\lambda,\xi) & C^T \\ B_2^T(\lambda,\xi)P & -\gamma I & D_2^T \\ C & D_2 & -\gamma I \end{bmatrix} < 0 \tag{32}$$

Then, left and right multiply $diag(\,P^{-1} \quad I \quad I\,)$ of (32) and gain (33) where $Q = P^{-1}$

$$\begin{bmatrix} A(\lambda,\xi)Q + QA^T(\lambda,\xi) & B_2(\lambda,\xi) & QC^T \\ B_2^T(\lambda,\xi) & -\gamma I & D_2^T \\ CQ & D_2 & -\gamma I \end{bmatrix} < 0. \tag{33}$$

$$\begin{aligned} U_{Q,i} &= \begin{bmatrix} B_n^T\Lambda_i & -I + D_{mn}^T\Lambda_i & D_{yn}^T\Lambda_i & 0\end{bmatrix}\\ \Omega_{Q,i} &= \begin{bmatrix} Q\underline{A}^T + \underline{A}Q + B_u(KQ)_i + (KQ)_i^TB_u^T & QC_m^T + (KQ)_i^TD_{mu}^T & QC_y^T + (KQ)_i^TD_{yu}^T & B_w \\ C_mQ + D_u(KQ)_i^T & 0 & 0 & D_{mw} \\ C_yQ_i + D_{yu}(KQ)_i^T & 0 & -\gamma I & D_{yw} \\ B_w^T & D_{mw}^T & D_{yw}^T & -\gamma I \end{bmatrix}\\ W_{Q,i} &= \frac{1}{2}\begin{bmatrix} C_m + D_{yu}K_i & D_{mn}\Lambda_i + I & D_{mw} & 0\end{bmatrix},\\ E &= \{Co\{A_i, i = 1, 2, \ldots, k\} + Co\{B_1, i = 1, 2, \ldots, k\}\, Co\{K_i, i = 1, 2, \ldots, k\}\}FC \end{aligned} \tag{28, 29}$$

Furthermore, we can derive (34)

$$\begin{bmatrix} A(\lambda,\xi)Q + QA^T(\lambda,\xi) & QC^T & B_2(\lambda,\xi) \\ CQ & -\gamma I & D_2^T \\ B_2^T(\lambda,\xi) & D_2 & -\gamma I \end{bmatrix} < 0. \quad (34)$$

The derivation (31)-(34) shows that system (35) satisfies Lemma 2 (bounded real Theorem)

$$\begin{cases} \dot{x} = A^T(\lambda,\xi)x + C^T w \\ y = B_2^T(\lambda,\xi)x + D_2^T w. \end{cases} \quad (35)$$

In addition, we can deduce (37), as shown at the bottom of this page, by (36), as shown at the bottom of this page.

Hence, its LFR form is as follows

$$\begin{cases} \dot{x} = \underline{A}^T x + C_m^T n + C_y^T w \\ m = B_n^T x + D_{mn}^T n + D_{yn}^T w \\ y = B_w^T x + D_{mw}^T n + D_{yw}^T w \\ n = \Lambda(\lambda,\xi)m \\ \Lambda(\lambda,\xi) = diag(\lambda I_1, \xi I_2). \end{cases} \quad (38)$$

Substitute System (38) into Lemma 3 with the selection of G, H, J in [28] as (39)

$$\begin{aligned} G &= \frac{1}{2}C_m^T M \\ H &= \frac{1}{2}M(D_{mn}\Lambda(\lambda,\xi) + I) \\ J &= \frac{1}{2}MD_{mw}, \end{aligned} \quad (39)$$

and then, the variables in (27) can be obtained as shown in (40)

$$\begin{aligned} U_{Q,i} &= \begin{bmatrix} B_n^T\Lambda_i & -I + D_{mn}^T\Lambda_i & D_{yn}^T\Lambda_i & 0 \end{bmatrix} \\ \Omega_Q &= \begin{bmatrix} Q\underline{A}^T + \underline{A}Q & QC_m^T & QC_y^T & B_w \\ C_mQ & 0 & 0 & D_{mw} \\ C_yQ & 0 & -\gamma I & D_{yw} \\ B_w^T & D_{mw}^T & D_{yw}^T & -\gamma I \end{bmatrix} \\ W_{Q,i} &= \frac{1}{2}\begin{bmatrix} C_m & D_{mn}\Lambda_i + I & D_{mw} & 0 \end{bmatrix}. \end{aligned} \quad (40)$$

Thus far, a form of linear inequality that can be directly used by the LMI toolbox in MATLAB is obtained.

Substitute the H_∞ control rate $u = Kx$ in the LFR model (25) of the morphing aircraft, and obtain (41)

$$\begin{cases} \dot{x} = (\underline{A} + B_uK)x + B_n n + B_w w \\ m = (C_m + D_{mu}K)x + D_{mn}n + D_{mw}w \\ y = (C_y + D_{yu}K)x + D_{yn}n + D_{yw}w \\ n = \Lambda(\lambda,\xi)m \\ \Lambda(\lambda,\xi) = diag(\lambda I_1, \xi I_2). \end{cases} \quad (41)$$

The LMI condition (27)-(28) is obtained by (40) and (41) to satisfy the secondary H_∞ performance. According to Lemma 1, the feedback matrix of LFR system (18) can be taken as

$$Co\{K_i, i = 1, 2, \ldots, k\} := \left\{ \sum_{i=1}^{k} \alpha_i K_i | \alpha_i \geq 0, \sum_{i=1}^{k} \alpha_i = 1 \right\}. \quad (42)$$

The state equation of the closed-loop system after the feedback matrix $K(\lambda,\xi)$ is introduced at this time as (43)

$$A_d(\lambda,\xi) = A(\lambda,\xi) + B(\lambda,\xi)K(\lambda,\xi) \quad (43)$$

Matrix $A_d(\lambda,\xi)$ can be arbitrarily assigned, which is expressed in the controllable canonical form in (44), as shown at the bottom of this page, where $a_1, a_2 \ldots a_7$ are the functions of λ, ξ and $s^6 + a_7 s^5 + \ldots + a_2 s + a_1 = 0$ is the desired closed-loop characteristic equation. At this point, the closed-loop model of the LPV system based on the H_∞ controller has been successfully built.

Third, we chose the integral sliding surface for the same closed-loop poles with the LFR-H_∞ controller.

Remark 2: To derive the equivalent part of the control law when the system response converges to the sliding surface, assume that there is no uncertainty in the coefficient matrix of the system and interference, that is, $\Delta A = 0$ and $w = 0$.

The integral sliding surface selection is as shown in (26). Assuming that the system can converge to the integral sliding

$$\begin{bmatrix} A(\lambda,\xi) & B_2(\lambda,\xi) \\ C & D_2 \end{bmatrix} = \begin{bmatrix} \underline{A} & B_w \\ C_y & D_{yw} \end{bmatrix} + \begin{bmatrix} B_n \\ D_{yn} \end{bmatrix} \times \Lambda(\lambda,\xi)(I - D_{mn}\Lambda(\lambda,\xi))^{-1} \begin{bmatrix} C_m & D_{mw} \end{bmatrix} \quad (36)$$

$$\begin{bmatrix} A^T(\lambda,\xi) & C^T \\ B_2^T(\lambda,\xi) & D_2^T \end{bmatrix} = \begin{bmatrix} \underline{A}^T & C_y^T \\ B_w^T & D_{yw}^T \end{bmatrix} + \begin{bmatrix} C_m^T \\ D_{mw}^T \end{bmatrix} \times \Lambda(\lambda,\xi)(I - D_{mn}^T\Lambda(\lambda,\xi))^{-1} \begin{bmatrix} B_n^T & D_{yn}^T \end{bmatrix} \quad (37)$$

$$A_d(\lambda,\xi) = \begin{bmatrix} 0 & 1 & 0 & 0 & 0 & 0 & 0 \\ 0 & 0 & 1 & 0 & 0 & 0 & 0 \\ 0 & 0 & 0 & 1 & 0 & 0 & 0 \\ 0 & 0 & 0 & 0 & 1 & 0 & 0 \\ 0 & 0 & 0 & 0 & 0 & 1 & 0 \\ 0 & 0 & 0 & 0 & 0 & 0 & 1 \\ -a_1(\lambda,\xi) & -a_2(\lambda,\xi) & -a_3(\lambda,\xi) & -a_4(\lambda,\xi) & -a_5(\lambda,\xi) & -a_6(\lambda,\xi) & -a_7(\lambda,\xi) \end{bmatrix} \quad (44)$$

surface in finite time, the linear equivalent control u_{eq} can make the first derivative of the sliding surface $\dot{s} = 0$

$$\begin{aligned}\dot{s} &= -E(\lambda,\xi)\dot{x} + Fe \\ &= -E(\lambda,\xi)\left[A(\lambda,\xi)x + B_1(\lambda,\xi)u_{eq} + B_2 w\right] + F(y-\bar{y}) \\ &= -E(\lambda,\xi)A(\lambda,\xi)x - E(\lambda,\xi)B_1(\lambda,\xi)u_{eq} \\ &\quad - E(\lambda,\xi)B_2(\lambda,\xi)w + FCx - F\bar{y} \\ &= (-E(\lambda,\xi)A(\lambda,\xi)+FC)x - E(\lambda,\xi)B_1(\lambda,\xi)u_{eq} \\ &\quad - E(\lambda,\xi)B_2(\lambda,\xi)w - F\bar{y} \\ &= 0. \end{aligned} \tag{45}$$

From (45) to (46),

$$\begin{aligned}u_{eq} = (E(\lambda,\xi)B_1(\lambda,\xi))^{-1}[(-E(\lambda,\xi)A(\lambda,\xi)+FC)x \\ - E(\lambda,\xi)B_2(\lambda,\xi)w - F\bar{y}].\end{aligned} \tag{46}$$

Substituting $u = u_{eq}$ in LPV model (20) and obtain (47)

$$\begin{aligned}\dot{x} &= [A(\lambda,\xi) + B_1(\lambda,\xi)(E(\lambda,\xi)B_1(\lambda,\xi))^{-1}(-E(\lambda,\xi)A(\lambda,\xi) \\ &\quad + FC)]x - B_1(\lambda,\xi)(E(\lambda,\xi)B_1(\lambda,\xi))^{-1}F\bar{y} \\ &= A_{eq}x - B_1(\lambda,\xi)(E(\lambda,\xi)B_1(\lambda,\xi))^{-1}F\bar{y}. \end{aligned} \tag{47}$$

At this point, the closed-loop system equation under the integral sliding mode controller is obtained.

Finally, to make the poles of system (47) under the action of the integral sliding mode controller equal to the that of the feedback matrix obtained by the LFR-H_∞ controller, the two closed-loop systems should have the same system matrix. Hence,

$$A_{eq}(\lambda,\xi) = A_d(\lambda,\xi), \tag{48}$$

which is

$$\begin{aligned}A(\lambda,\xi) + B_1(\lambda,\xi)(E(\lambda,\xi)B_1(\lambda,\xi))^{-1} \\ \times(-E(\lambda,\xi)A(\lambda,\xi) + FC) \\ = A(\lambda,\xi) + B_1(\lambda,\xi)K(\lambda,\xi).\end{aligned} \tag{49}$$

Applying (49), we can obtain (50):

$$E(\lambda,\xi) = (A(\lambda,\xi) + B_1(\lambda,\xi)K(\lambda,\xi))^{-1}FC. \tag{50}$$

By Lemma 1, $E(\lambda,\xi)$ can be chosen as the polytopic form (51)

$$\begin{aligned}E = \{Co\{A_i, i = 1,2,\ldots,k\} + Co\{B_1, i = 1,2,\ldots,k\} \\ \cdot Co\{K_i, i = 1,2,\ldots,k\}\}FC.\end{aligned} \tag{51}$$

When (51) is satisfied, the closed-loop system composed of the integral sliding mode controller obtains all the desired poles of the LFR-H_∞ controller. That is, the two controllers have the same effect without parameter perturbation. Therefore, the integral sliding mode switch surface (26) of this part is implemented.

This completes the proof.

B. SELF-ADAPTION INTEGRAL SLIDING MODE CONTROL RATE DESIGN AND STABILITY ANALYSIS

On the basis of Section IV.A, an integral sliding mode approaching the control rate with finite-time convergence is designed based on the idea of parameter dependence. Hence, the uncertain LPV system can converge to the sliding mode switching surface $s = 0$ in finite time under this control rate and subsequently maintain the sliding mode motion.

In this part, by using the Lyapunov stability proof method, we prove the stability of the system based on the LFR-H_∞ controller first to confirm the effectiveness of its design. Then, we prove the stability of the system under the action of the integral sliding mode controller designed based on the LFR-H_∞ controller.

Theorem 2: Suppose the integral sliding surface exists that satisfies the conditions in Theorem 1. The uncertain LPV system converges to the switching surface in finite time under the effect of the sliding mode approaching the control rate (52)

$$\begin{aligned}u &= -(EB_1)^{-1}EAx + (EB_1)^{-1}Fe \\ &\quad + (EB_1)^{-1}\left[\mu + \Delta\hat{A}||E||||x|| + \hat{w}||EB_2||\right]sign(s),\end{aligned} \tag{52}$$

where

$$\begin{cases} A = Co\{A_i, i = 1,2,\ldots,k\} \\ B_1 = Co\{B_{1i}, i = 1,2,\ldots,k\} \\ E = Co\{E_i, i = 1,2,\ldots,k\}, \end{cases} \tag{53}$$

$$sign(s) = \delta s. \tag{54}$$

$\Delta\hat{A}$ and $\hat{w}$ are the estimated values of ΔA and ω satisfying $\Delta\hat{A}(0) = 0$, $\hat{w}(0) = 0$, respectively. In addition, $\mu, \delta > 0$ are adjustable gain parameters; $sign(\bullet)$ is the approximate function of the switching function to improve the chattering problem. In addition, the adaptive rates are as follows

$$\begin{cases} \dot{\Delta\hat{A}} = \eta||s(t)||||Ex|| \\ \dot{\hat{w}} = \varepsilon||s(t)||||EB_2|| \end{cases}. \tag{55}$$

Assumption 1: The upper bounds of ΔA and $w(t)$ are unknown.

Proof: First, it is proven that the LPV system (20) is stable under the action of the LFR-H_∞ controller. The parameter-dependent Lyapunov function is chosen as (56)

$$V_{H_\infty} = x^T Q(\lambda,\xi)x \tag{56}$$

$$\begin{aligned}\dot{V}_{H_\infty} &= x^T Q(\lambda,\xi)\left[A(\lambda,\xi)x + B(\lambda,\xi)K(\lambda,\xi)x\right] + \left[x^T A^T(\lambda,\xi) + x^T K(\lambda,\xi)^T B(\lambda,\xi)^T\right]Q(\lambda,\xi)x \\ &= x^T\left[Q(\lambda,\xi)A(\lambda,\xi) + Q(\lambda,\xi)B(\lambda,\xi)K(\lambda,\xi) + A^T(\lambda,\xi)Q(\lambda,\xi) + K(\lambda,\xi)^T B(\lambda,\xi)^T Q(\lambda,\xi)\right]x \\ &= x^T\left[Q(\lambda,\xi)A(\lambda,\xi) + (K(\lambda,\xi)Q(\lambda,\xi))B(\lambda,\xi) + A^T(\lambda,\xi)Q(\lambda,\xi) + (K(\lambda,\xi)Q(\lambda,\xi))^T B(\lambda,\xi)^T\right]x \end{aligned} \tag{58}$$

In (56), Q is the inverse matrix of the Lyapunov matrix. Further,

$$\begin{aligned}\dot{V}_{H_\infty} &= x^T Q(\lambda,\xi)\dot{x} + \dot{x}^T Q(\lambda,\xi)x \\ &= x^T Q(\lambda,\xi)\left[A(\lambda,\xi)x + B(\lambda,\xi)u\right] \\ &\quad + \left[x^T A^T(\lambda,\xi) + u^T B(\lambda,\xi)^T\right] Q(\lambda,\xi)x, \end{aligned} \tag{57}$$

Insert $u = Kx$ into (57) to obtain (58), as shown at the bottom of the previous page.

By Lemma 1

$$\dot{V}_{H_\infty} \triangleq x^T \left[QA + (KQ)B + A^T Q + (KQ)^T B^T\right] x, \tag{59}$$

where

$$\begin{cases} Q = Co\{Q_i, i = 1, 2, \ldots, k\} \\ (KQ) = Co\left\{(KQ)_i, i = 1, 2, \ldots, k\right\}. \end{cases} \tag{60}$$

It is deduced from Lemma 1 and Lemma 4 that

$$QA + (KQ)B + A^T Q + (KQ)^T B^T < 0. \tag{61}$$

Hence,

$$\dot{V}_{H_\infty} < 0. \tag{62}$$

By (62), the system is stable under the LFR-H_∞ controller. Therefore, the integral sliding mode controller designed based on the LFR-H_∞ controller is reasonable and effective. Next, it is proven that the integral sliding mode controller designed in this paper can make the uncertain LPV system (20) converge to the sliding mode switching surface in a limited amount of time.

$s(t) = 0$ is chosen as the sliding mode switching surface, and the parameter-dependent Lyapunov function is chosen as follows:

$$V = \frac{1}{2}s^T(t)s(t) + \frac{1}{2\eta}\Delta\tilde{A}^2 + \frac{1}{2\varepsilon}\tilde{w}^2. \tag{63}$$

where

$$\begin{cases} \Delta\tilde{A} = \Delta\hat{A} - \Delta A \\ \tilde{w} = \hat{w} - w \end{cases} \tag{64}$$

are the errors between the estimated values and the true values.

Substituting the control rate derived in (65) into (63), we obtain (66), as shown at the bottom of this page.

$$\begin{cases} u = -(E(\lambda,\xi)B_1(\lambda,\xi))^{-1}E(\lambda,\xi)A(\lambda,\xi)x \\ \quad +(E(\lambda,\xi)B_1(\lambda,\xi))^{-1}Fe \\ \quad +(E(\lambda,\xi)B_1(\lambda,\xi))^{-1}f(\lambda,\xi)sign(s) \\ f(\lambda,\xi) = \mu + \Delta\hat{A}||E(\lambda,\xi)||||x|| + \hat{\omega}||E(\lambda,\xi)B_2(\lambda,\xi)||, \end{cases} \tag{65}$$

The inequalities in (67), as shown at the bottom of this page, are derived from the following relationship:

$$\bullet^T sign(\bullet) = \sum_{i=1}^{m} |\bullet_i| \geq \sqrt{\sum_{i=1}^{m} |\bullet_i|^2} = ||\bullet||. \tag{68}$$

Additionally, by Lemma 1, (65) can be chosen to be in the form of (52).

At this point, Theorem 2 is proven.

Remark 3: In the control law in (52), the chattering problem in the sliding mode controller is suppressed by replacing $\delta\cdot(\bullet)$

$$\begin{aligned}\dot{V} &= s^T(t)\dot{s}(t) + \frac{1}{\eta}\Delta\tilde{A}\Delta\dot{\hat{A}} + \frac{1}{\varepsilon}\tilde{w}\dot{\hat{w}} \\ &= s^T(t)\left(-E(\lambda,\xi)\dot{x} + Fe\right) + \frac{1}{\eta}\Delta\tilde{A}\Delta\dot{\hat{A}} + \frac{1}{\varepsilon}\tilde{w}\dot{\hat{w}} \\ &= s^T(t)\left[-E(\lambda,\xi)\left(A(\lambda,\xi)x + B_1(\lambda,\xi)u + B_2 w + \Delta Ax\right) + Fe\right] + \frac{1}{\eta}\Delta\tilde{A}\Delta\dot{\hat{A}} + \frac{1}{\varepsilon}\tilde{w}\dot{\hat{w}} \\ &= s^T(t)\left[(-\mu - \Delta\hat{A}||E(\lambda,\xi)x|| - \hat{w}||EB_2(\lambda,\xi)||)sign(s) - EB_2(\lambda,\xi)w - E(\lambda,\xi)\Delta Ax\right] + \frac{1}{\eta}\Delta\tilde{A}\Delta\dot{\hat{A}} + \frac{1}{\varepsilon}\tilde{w}\dot{\hat{w}} \\ &= s^T(t)\left[(-\mu - \Delta\hat{A}||E(\lambda,\xi)x|| - \hat{w}||EB_2(\lambda,\xi)||)sign(s) - EB_2(\lambda,\xi)w - E(\lambda,\xi)\Delta Ax\right] \\ &\quad + ||s||||E(\lambda,\xi)x|||\Delta\tilde{A} + ||s||||EB_2(\lambda,\xi)||\tilde{w} \\ &= s^T(t)\left[(-\mu - \Delta\hat{A}||E(\lambda,\xi)x|| - \hat{w}||EB_2(\lambda,\xi)||)sign(s) - EB_2(\lambda,\xi)w - E(\lambda,\xi)\Delta Ax\right] \\ &\quad + ||s||||E(\lambda,\xi)x|||(\Delta\hat{A} - \Delta A) + ||s||||EB_2(\lambda,\xi)||(\hat{w} - w). \end{aligned} \tag{66}$$

$$\begin{aligned}\dot{V} &\leq ||s||\left[(-\mu - \Delta\hat{A}||E(\lambda,\xi)x|| - \hat{w}||EB_2(\lambda,\xi)||) - EB_2(\lambda,\xi)w - E(\lambda,\xi)\Delta Ax\right] \\ &\quad + ||s||||E(\lambda,\xi)x|||(\Delta\hat{A} - \Delta A) + ||s||||EB_2(\lambda,\xi)||(\hat{w} - w) \\ &\leq ||s||\left[(-\mu - \Delta\hat{A}||E(\lambda,\xi)x|| - \hat{w}||EB_2(\lambda,\xi)||) + ||EB_2(\lambda,\xi)||w + ||E(\lambda,\xi)x||\Delta A\right] \\ &\quad + ||s||||E(\lambda,\xi)x|||(\Delta\hat{A} - \Delta A) + ||s||||EB_2(\lambda,\xi)||(\hat{w} - w) \\ &\leq -\mu||s|| \\ &\leq 0 \end{aligned} \tag{67}$$

with $sign(\bullet)$, where δ is an adjustable scalar. Then, tune the gain parameters μ, δ, η, ε to obtain better robust performance and reduce the chattering in the simulation.

V. SIMULATION

To verify the effectiveness and advantages of the self-adaptive integrated sliding mode controller designed in this paper, two types of simulation experiments are carried out in this part. First, the effects of the integral sliding mode controller with self-adaption are compared with that of the integral sliding mode controller, sliding mode controller and LFR-H_∞ controller when the model parameters are not perturbed. Second, the advantage in the anti-interference of the self-adaption integral sliding mode controller is demonstrated by comparison with results of the LFR-H_∞ controller when the aerodynamic parameters have different degrees of perturbation.

First, we use the TP toolbox in MATLAB to decompose the LPV system (20) to a polytopic model (22) with $4 \times 3 = 12$ vertices. For the two time-varying parameters λ, ξ in the LPV system, take 4 singular values in the λ direction and 3 singular values in the ξ direction in consideration of the computational complexity and accuracy. The specific system matrix and parameters at the vertices are not listed in this paper. Second, the LPV model is transformed into the LTI system form (25) by an LFR transformation with the LMI toolbox in MATLAB. At this point, all the mathematical model results of the morphing aircraft required by the simulation in this paper are obtained. The specific simulation results are shown in the appendix.

Here, the desired performance is selected as $\gamma = 10$ to design the feedback matrix $Co\{K_{12}, i = 1, 2, \ldots, 12\}$ in Theorem 1 by using the YALMIP interface with the SDP solver SeduMi toolbox in MATLAB. $Co\{K_{12}, i = 1, 2, \ldots, 12\}$ is calculated as (69), as shown at the bottom of this page. In addition, for the convenience of parameter debugging, F in the integral sliding surface as described in (26) is chosen as the full-rank identity matrix

$$F = I_{7\times 7}. \tag{70}$$

Other adjustable constants in the integral sliding mode control law (52) and adaptive rate (54) are selected as (71)

$$\begin{aligned} \mu &= 2.5 \\ \delta &= 200 \\ \eta &= 0.15 \\ \varepsilon &= 0.10. \end{aligned} \tag{71}$$

The simulation considers the following conditions in Fig. 5. At the initial time, the aircraft is in the full-length and zero-sweep state ($\lambda = 0, \xi = 0.8$) with a fixed speed and height. The morphing aircraft moves to a large sweep angle and full wing contraction ($\lambda = 1, \xi = 0$) in 10 seconds, gradually starting from the tenth second. The morphing aircraft is in a constant-speed and constant-height flight state. The flight conditions are selected as $h_0 = 9144\ m$ and $V_0 = 0.5\ Mach$ ($V_0 \approx 170.15\ m/s$). The morphing aircraft completes the variant process in a state of uniform linear flight.

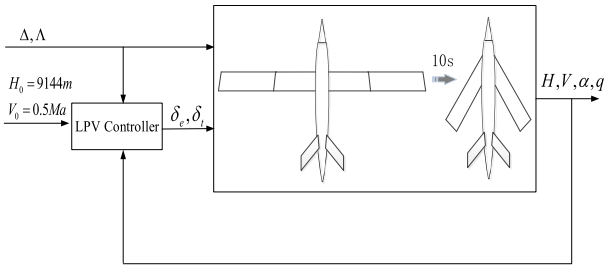

FIGURE 5. Morphing process in the simulation.

TABLE 3. Trimming state under typical shapes of the morphing aircraft.

	$\lambda = 0, \xi = 0.8$	...	$\lambda = 1, \xi = 0$
H_{trim}	$9144\ m$	...	$9144\ m$
V_{trim}	$0.5\ Mach$	...	$0.5\ Mach$
α_{trim}	$-0.99°$	...	$-1.29°$
q_{trim}	$0°/s$	...	$0°/s$
$\delta_{e_{trim}}$	$2.16°$	...	$-2.00°$
$\delta_{T_{trim}}$	16.75%	...	12.65%

In this morphing scenario, two cases were evaluated. In case 1, the integral sliding mode controller and the self-adaptive integral sliding mode controller designed in this paper are compared with the LFR-H_∞ controller and finite time convergence sliding mode controller developed in [7] while assuming that the LPV model of the morphing aircraft (20) is established accurately (no disturbance or model perturbation). In case 2, the adaptive integral sliding mode controller is compared with the LFR-H_∞ controller with different degrees of perturbation for aerodynamic coefficients and other parameters.

Fig. 6 and Fig. 7 are comparison simulation curves of the four controllers in case 1, where AISMC, ISMC, SMC and LFR-H_∞ represent the self-adaptive integral sliding mode controller, integral sliding mode controller, sliding mode controller and LFR-H_∞ controller, respectively. The equilibrium state of the morphing aircraft before variant implementation is shown in Table 3.

The simulation results of case 1 show that the four controllers can maintain the speed and height stability

$$Co\{K_{12}, i=1, \ldots, 12\} = \begin{bmatrix} -24.71 & -46768.41 & 653.16 & 55604.98 & 1624.23 & -159.28 & 4330.60 \\ -260.45 & -342399.94 & 4775.14 & 407138.43 & 11876.38 & -2454.45 & 31672.12 \end{bmatrix} \tag{69}$$

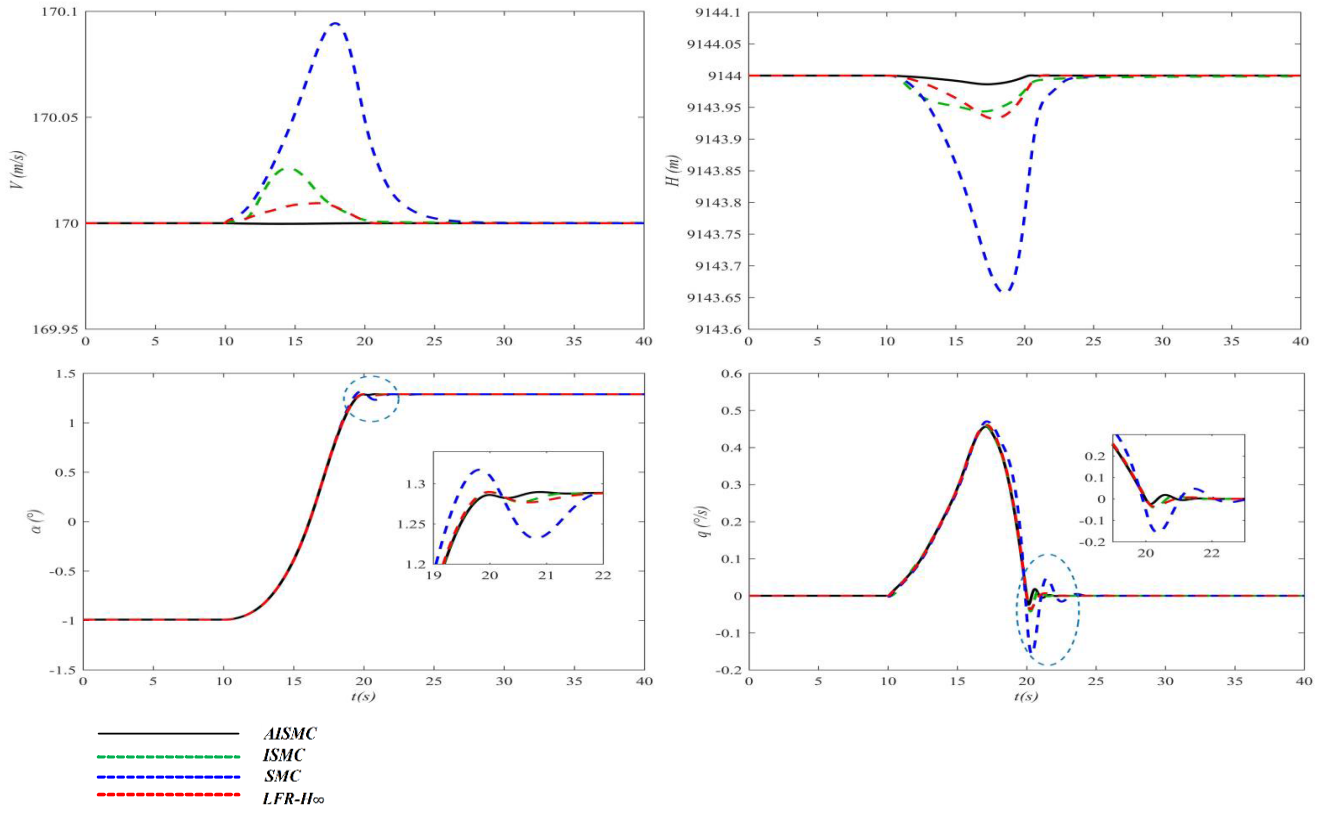

FIGURE 6. Case 1: Closed-loop response of the four controllers in the morphing process without perturbation.

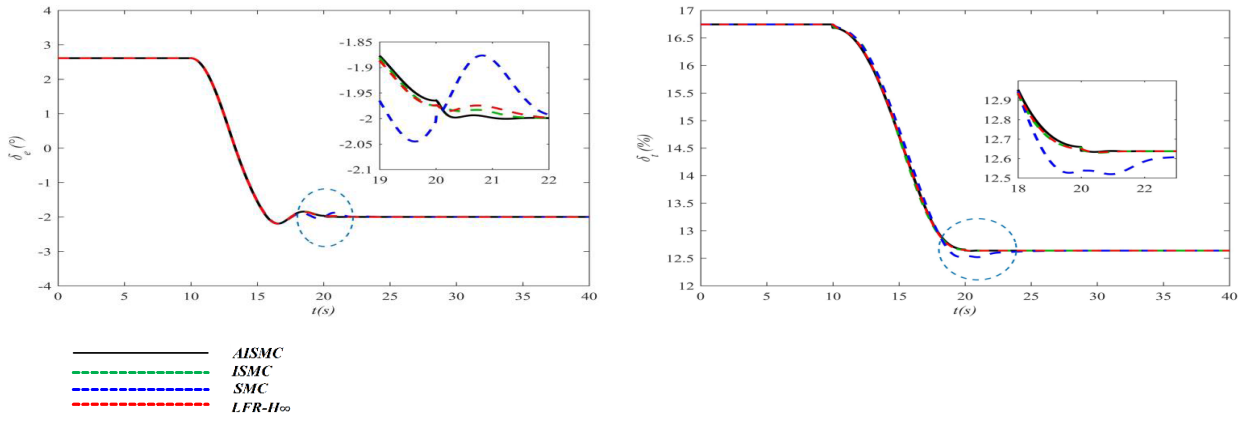

FIGURE 7. Case 1: Closed-loop outputs of the four controllers in the morphing process without perturbation.

requirements of the morphing aircraft in the short-time and large-scale morphing process. While the control quality of the integral sliding mode controller is improved compared to that of the sliding mode controller and LFR-H_∞ controller, the addition of the adaptive rate further suppresses the fluctuations in the speed and height of the morphing process. Under the action of the adaptive integral sliding mode controller, $|\Delta V_{\max}| < 0.0004$, $|\Delta H_{\max}| < 0.014$. In this simulation, after the variant implementation is completed, the speed and height of the aircraft are consistent with those before morphing, where there are no static differences.

Fig. 7 shows the output curves of controllers during morphing. As the area of wings decreases, the angle of attack is increased to improve the lift. As the angle of attack increases, the elevator angle decreases. The increase in the sweep angle and the reduction in the wing area cause the resistance of the aircraft to be reduced. Therefore, the throttle opening is reduced. In addition, the output curves of the integral sliding

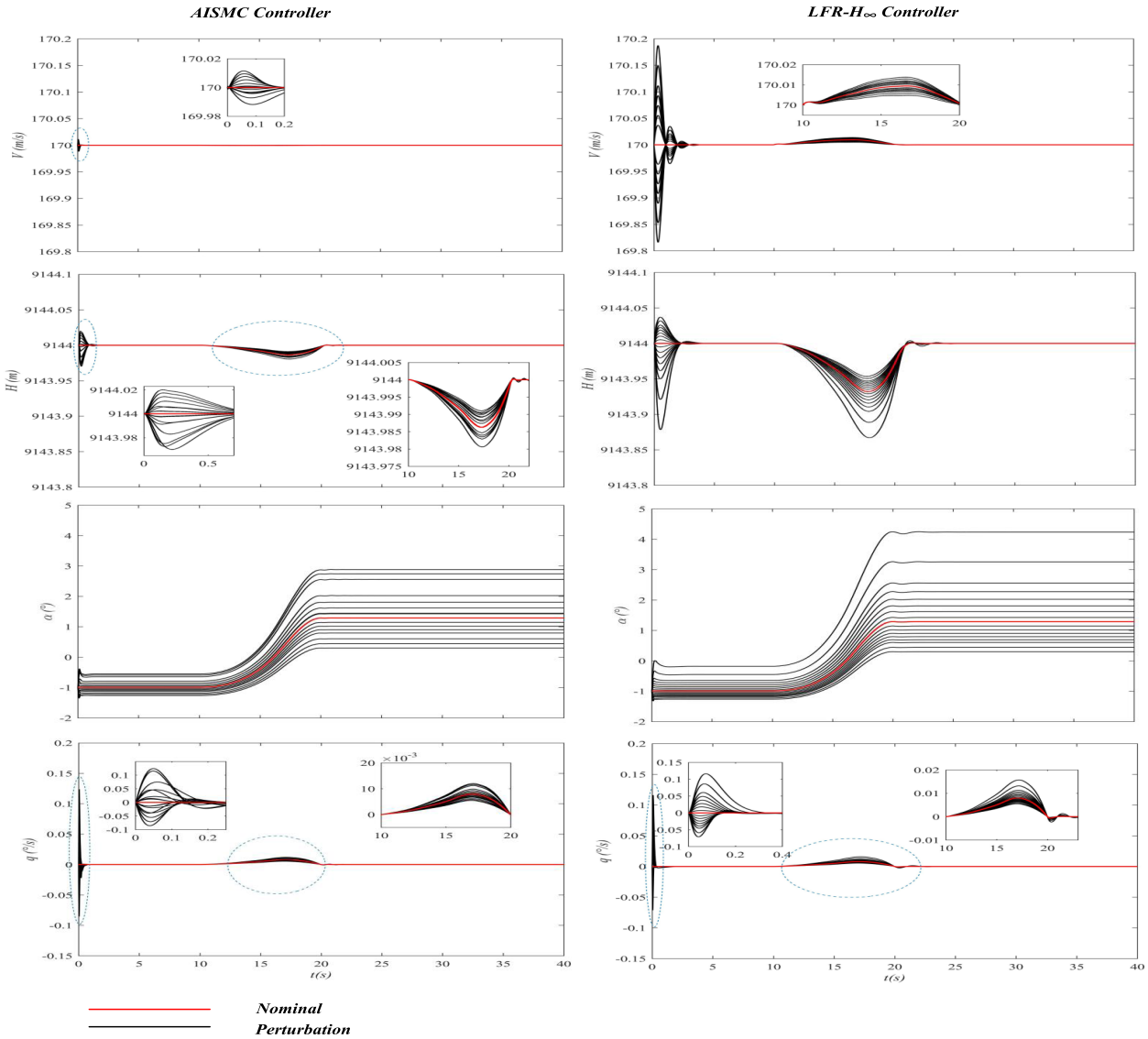

FIGURE 8. Case 2: Closed-loop response of the AISMC controller and LFR-H_∞ controller in the morphing process with perturbations.

mode controller exhibit no high-frequency oscillation, which indicates that the shaking is well suppressed.

The mathematical model of the morphing aircraft has strong nonlinearity and uncertainty; hence, the model is difficult to establish accurately, which places extremely high requirements on the robustness of the controller. The nondeterministic parameters in case 2 are designed in (72)

$$\begin{aligned} \Delta C_L = \Delta C_D = \Delta C_M \\ = 0, \quad \pm 10\%, \pm 20\%, \pm 30\%, \pm 40\%, \pm 50\% \\ \Delta Q = 0, \quad \pm 15\%, \pm 25\% \\ \Delta m_t = 0, \quad \pm 5\%. \end{aligned} \tag{72}$$

In what follows, 17 separate simulation experiments are evaluated with different perturbation parameters for the two controllers. The closed-loop responses with perturbations of the AISMC controller and LFR-H_∞ controller are shown in Fig. 8 during the morphing process. In addition, the outputs from two controllers are shown in Fig. 9.

The curves in Fig. 8 show that both controllers can converge the flight speed and height to given values when the aircraft exhibits perturbations during morphing. The simulation results of case 2 show that the robustness of the adaptive integral sliding mode controller is better than that of the conventional H_∞ controller. On the one hand, the static characteristics of the system have been improved. With perturbations in the model of the aircraft, the output variations of the adaptive integral sliding mode controller are (73)

$$\begin{cases} \left|\Delta V_{AISMC\_perturbation}\right|_{\max} \approx 0.01 m/s \\ \left|\Delta H_{AISMC\_perturbation}\right|_{\max} \approx 0.02 m \\ \left|\Delta \alpha_{AISMC\_perturbation}\right|_{\max} \approx 3^\circ \\ \left|\Delta q_{AISMC\_perturbation}\right|_{\max} \approx 0.13^\circ/s. \end{cases} \tag{73}$$

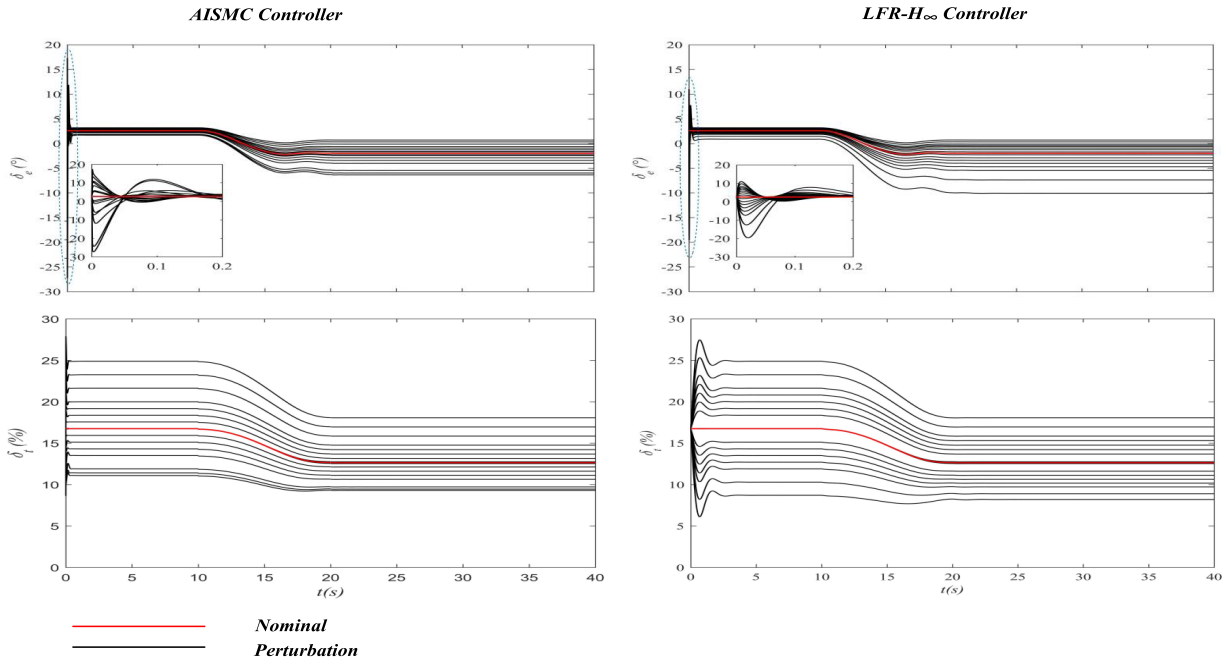

FIGURE 9. Case 2: Closed-loop AISMC controller and LFR-H_∞ controller outputs in the morphing process with perturbations.

Under the same conditions, the fluctuations of the LFR-H_∞ controller are (74)

$$\begin{cases} \left|\Delta V_{H_\infty\_perturbation}\right|_{\max} \approx 0.20m/s \\ \left|\Delta H_{H_\infty\_perturbation}\right|_{\max} \approx 0.15m \\ \left|\Delta \alpha_{H_\infty\_perturbation}\right|_{\max} \approx 4.50^\circ \\ \left|\Delta q_{H_\infty\_perturbation}\right|_{\max} \approx 0.13^\circ/s. \end{cases} \tag{74}$$

On the other hand, the dynamic characteristics of the system under ASIMC have also been ameliorated. The adjustment times under the action of the controllers are (75)

$$\begin{aligned} t_{s(AISMC\_perturbation)} &\approx 1.2s \\ t_{s(H_\infty\_perturbation)} &\approx 3.8s. \end{aligned} \tag{75}$$

In the case of the same degree of perturbation, the integral sliding mode controller causes the actuator to activate by a small amount; hence, the stability of the variant process can be ensured over a larger perturbation range, and the antisaturation capability is stronger.

VI. CONCLUSION

This paper researches an adaptive integral sliding mode controller of the LPV model by exploring a morphing aircraft with variable sweep angles and variable lengths, ensuring the stability of the morphing aircraft in the variant process.

First, the longitudinal dynamic mathematical model of a variant aircraft is established and transformed. In the first step, the longitudinal nonlinear model of the variant aircraft based on the Kane rigid body modeling method is linearized to obtain an LPV model with a bounded L_2 gain performance capable of describing its dynamic characteristics. In the second step, the LPV model is decomposed into a polytopic form using the polytopic characteristics of the LPV system. In the third step, the LFR transformation method is used to transform the LPV system into an equivalent LTI model in a special form where the time-varying parameter is used as a diagonal matrix in the feedback loop of the LTI system.

Second, the existence conditions of the integral sliding surface that can keep the variation process stable are derived. In the first step, an LFR-H_∞ controller based on the state feedback is derived from a directly applicable quadratic stability LMI condition for the LFR model. In the second step, the integral sliding mode surface with the same poles as the closed-loop system under the action of LFR-H_∞ controller is obtained from the pole configuration method.

Then, the adaptive laws are used to estimate the perturbation parameters and interference in the system to improve the robustness of the uncertain system. Furthermore, the designed AISMC controller can drive the closed-loop system to converge to the switch integral sliding mode surface within a finite time under the stability analysis of the parameter-dependent Lyapunov function.

Finally, digital simulation proves that AISMC makes the morphing process maintain better nominal performance and robustness with uncertainty in the nonlinear model.

The adaptive integral sliding mode controller design method proposed in this paper can be extended to cover a wide range of general uncertain LPV model.

APPENDIX

A. THE SPECIFIC DEFINITIONS OF MATRICES IN THE LFR MODEL OF THE MORPHING AIRCRAFT

$$\underline{A} = \begin{bmatrix} -0.0229 & 4.5881 & 0 & -9.8000 & 0 & 0 & 0 \\ 0 & -2.5832 & 1 & 0 & 0 & 0 & 0 \\ 0 & -24.3367 & 0 & 0 & 0 & 0 & 0 \\ 0 & 0 & 1 & 0 & 0 & 0 & 0 \\ 0 & -170 & 0 & 170 & 0 & 0 & 0 \\ 1 & 0 & 0 & 0 & 0 & 0 & 0 \\ 0 & 0 & 0 & 0 & 1 & 0 & 0 \end{bmatrix} \tag{A.1}$$

$$B_u = \begin{bmatrix} 0.0191 & 0.1425 \\ -0.1189 & 0 \\ -14.3633 & 0 \\ 0 & 0 \\ 0 & 0 \\ 0 & 0 \\ 0 & 0 \end{bmatrix} \tag{A.2}$$

$$B_n = \begin{bmatrix} B_{n11} & B_{n12} & B_{n13} & B_{n14} \\ B_{n21} & B_{n22} & B_{n23} & B_{n24} \end{bmatrix}$$

$$\begin{cases} B_{n11} = B_{n21} = 0_{3\times 10} \\ B_{n12} = \begin{bmatrix} -0.0100 & -10.0991 & 2.1956 \\ -2.0022 & 0.0512 & 1.7958 \\ 0.0108 & 0.0658 & 335.5587 \end{bmatrix} \\ B_{n13} = B_{n23} = 0_{3\times 6} \\ B_{n14} = B_{n24} = 0_{3\times 1} \\ B_{n22} = 0_{3\times 3} \end{cases} \tag{A.3}$$

$$D_{yn} = 0_{2\times 23} \tag{A.4}$$

$$\Lambda(\lambda, \xi) = diag\left(\underbrace{\lambda \quad \cdots \quad \lambda}_{13} \underbrace{\xi \quad \cdots \quad \xi}_{10} \right) \tag{A.5}$$

$$C_y = \begin{bmatrix} 0 & 0 & 0 & 0 & 0 & 1 & 0 \\ 0 & 0 & 0 & 0 & 0 & 0 & 1 \end{bmatrix} \tag{A.6}$$

$$D_{yu} = 0_{2\times 2} \tag{A.7}$$

$$D_{yn} = 0_{2\times 23} \tag{A.8}$$

(A.9) as shown at the bottom of this page, and (A.10), as shown at the top of the next page.

$$C_m = \begin{bmatrix} C_{m11} & C_{m12} & C_{m13} & C_{m14} & C_{m15} & C_{m16} \\ C_{m21} & C_{m22} & C_{m23} & C_{m24} & C_{m25} & C_{m26} \end{bmatrix}^T$$

$$\begin{cases} C_{m11} = \begin{bmatrix} 0.0038 & 0.0091 & 0 \\ -0.0051 & 0.7896 & -2.0985 \end{bmatrix} \\ C_{m12} = \begin{bmatrix} 0.0060 & 0 & -0.0023 \\ 0.2912 & -0.1127 & 0.3233 \end{bmatrix} \\ C_{m13} = \begin{bmatrix} -0.0014 & 0.0073 & 0.0028 \\ 2.5817 & -0.6354 & -0.0723 \end{bmatrix} \\ C_{m14} = \begin{bmatrix} 0 & 0 & 0 & 0 \\ 1.2866 & 0.9941 & -0.2239 & -0.0566 \end{bmatrix} \\ C_{m15} = \begin{bmatrix} 1.6593 & -0.4958 & 0.0158 & 0.0226 & 0.0087 \\ -0.0194 & -0.0690 & -0.5841 & 0.0136 & -1.2486 \end{bmatrix} \\ C_{m16} = \begin{bmatrix} 0.0015 & 0.0017 & -0.0017 & 0 & 0 \\ 4.7739 & 3.5233 & -2.6249 & 0.0324 & 0 \end{bmatrix} \\ C_{m21} = C_{m22} = C_{m23} = 0_{3\times 5} \\ C_{m24} = 0_{4\times 5} \\ C_{m25} = 0_{5\times 5} \\ C_{m26} = 0_{5\times 5} \end{cases} \tag{A.9}$$

$$D_{mu} = \begin{bmatrix} D_{mu11} & D_{mu12} & D_{mu13} & D_{mu14} & D_{mu15} & D_{mu16} \end{bmatrix}^T$$
$$\begin{cases} D_{mu11} = \begin{bmatrix} -0.0211 & 0.0981 & -0.2739 \\ 0 & 0 & 0 \end{bmatrix} \\ D_{mu12} = \begin{bmatrix} 0.2245 & 2.9323 & 0.3906 \\ 0 & 0 & 0 \end{bmatrix} \\ D_{mu13} = \begin{bmatrix} -0.2593 & -0.2148 & 0.0051 \\ 0 & 0 & 0 \end{bmatrix} \\ D_{mu14} = \begin{bmatrix} 0.0128 & 0 & -0.0089 & -0.0024 \\ 0 & 0 & 0 & 0 \end{bmatrix} \\ D_{mu15} = \begin{bmatrix} -0.1638 & -0.5074 & 3.4027 & -0.3699 & -2.7967 \\ 0 & 0 & 0 & 0 & 0 \end{bmatrix} \\ D_{mu16} = \begin{bmatrix} 0.0618 & -0.3212 & 0.2666 & -0.0322 & 0 \\ 0 & 0 & 0 & 0 & 0 \end{bmatrix} \end{cases} \tag{A.10}$$

REFERENCES

[1] E. W. Pendleton, D. Bessette, P. B. Field, G. D. Miller, and K. E. Griffin, "Active aeroelastic wing flight research program: Technical program and model analytical development," *J. Aircraft*, vol. 37, no. 4, pp. 554–561, Aug. 2000.
[2] K. Bonnema and S. Smith, "AFTI/F-111 mission adaptive wing flight research program," in *Proc. 4th Flight Test Conf.*, Aug. 2012, p. 2118.
[3] J. N. Kudva, "Overview of the DARPA smart wing project," *J. Intell. Mater. Syst. Struct.*, vol. 15, no. 4, pp. 261–267, Apr. 2004.
[4] S. Barbarino, O. Bilgen, and R. M. Ajaj, "A review of morphing aircraft," *J. Intell. Mater. Syst. Struct.*, vol. 22, no. 9, pp. 823–877, 2011.
[5] G. Shujuan, "Research on cooperative control of the morphing aircraft," MA. dissertation, Nanjing Univ. Aeronaut. Astronaut., Nanjing, China, 2012.
[6] B. Obradovic and K. Subbarao, "Modeling of flight dynamics of morphing wing aircraft," *J. Aircr.*, vol. 48, no. 2, pp. 391–402, 2011.
[7] N. Wen, Z. Liu, Y. Sun, and L. Zhu, "Design of LPV-based sliding mode controller with finite time convergence for a morphing aircraft," *Int. J. Aerosp. Eng.*, vol. 2017, Dec. 2017, Art. no. 8426348.
[8] J. Zhang and S.-T. Wu, "Dynamic modeling and control for a morphing aircraft," in *Proc. 26th Chin. Control Decis. Conf.*, Changsha, China, May/Jun. 2014, pp. 3418–3425.
[9] R. Padhi, N. Unnikrishnan, X. Wang, and S. N. Balakrishnan, "A single network adaptive critic (SNAC) architecture for optimal control synthesis for a class of nonlinear systems," *Neural Netw.*, vol. 19, no. 10, pp. 1648–1660, 2006.
[10] N. Wilfred, A. Chakravarthy, G. S. Lakshmikanth, and J. E. Steck, "Single network adaptive critic (SNAC) design for a morphing aircraft," in *Proc. AIAA Guid., Navigat. Control Conf.*, Aug. 2012, p. 4614.
[11] N. Wilfred, G. S. Lakshmikanth, A. Chakravarthy, and J. E. Steck, "Single network adaptive critic (SNAC) architecture for optimal tracking control of a morphing aircraft during a pull-up maneuver," in *Proc. AIAA Guid., Navigat. Control Conf.*, USA, vol. 14, Aug. 2013, p. 5003.
[12] T. M. Seigler, D. A. Neal, and D. Inman, "Dynamic modeling of large-scale morphing aircraft," in *Proc. 47th AIAA/ASME/ASCE/AHS/ASC Struct., Struct. Dyn. Mater. Conf.*, May 2006, pp. 3668–3678.
[13] T. M. Seigler and D. A. Neal, "Analysis of transition stability for morphing aircraft," *J. Guid. Control Dyn*, vol. 32, no. 6, pp. 1947–1954, Nov./Dec. 2009.
[14] N. Gandhi, A. Jha, J. Monaco, T. Seigler, D. Ward, and D. Inman, "Intelligent control of a morphing aircraft," in *Proc. 46th AIAA/ASME/ASCE/AHS/ASC Struct., Struct. Dyn. Mater. Conf.*, Apr. 2007, pp. 18–21.
[15] W. Tong, W. Qing, J. Weilai, and D. Chaoyang, "Gain schedule control of morphing vehicle based on switched polytopic system (in Chinese)," *J. Beijing Univ. Aeronaut. Astronaut. Astronaut.*, vol. 40, pp. 75–79, May 2014.
[16] Q. Wang, T. Wang, D.-L. Hou, and C.-Y. Dong, "Robust LPV control for morphing vehicles via velocity-based linearization (in Chinese)," *Syst. Eng. Electron.*, vol. 36, no. 6, pp. 1130–1136, Jun. 2014.
[17] D. H. Baldelli, D.-H. Lee, R. S. S. Peña, and B. Cannon, "Modeling and control of an aeroelastic morphing vehicle," *J. Guid., Control, Dyn.*, vol. 31, no. 6, pp. 1687–1699, Nov./Dec. 2008.
[18] T. Yue, L. Wang, and J. Ai, "Gain self-scheduled H_∞ control for morphing aircraft in the wing transition process based on an LPV model," *Chin. J. Aeronaut.*, vol. 26, no. 4, pp. 909–917, Aug. 2013.
[19] J.-L. Chang, "Dynamic output integral sliding-mode control with disturbance attenuation," *IEEE Trans. Autom. Control*, vol. 54, no. 11, pp. 2653–2658, Nov. 2009.
[20] H. H. Choi, "Variable structure control of dynamical systems with mismatched norm-bounded uncertainties: An LMI approach," *Int. J. Control*, vol. 74, no. 13, pp. 1324–1334, Jan. 2001.
[21] J.-C. Juang and C.-M. Lee, "Design of sliding mode controllers with bounded L_2 gain performance: An LMI approach," *Int. J. Control*, vol. 78, no. 9, pp. 647–661, Jun. 2005.
[22] X. Hu, L. Wu, C. Hu, and H. Gao, "Adaptive sliding mode tracking control for a flexible air-breathing hypersonic vehicle," *J. Franklin Inst.*, vol. 349, no. 2, pp. 559–577, 2012.
[23] H. Alwi, C. Edwards, and A. Marcos, "Fault reconstruction using a LPV sliding mode observer for a class of LPV systems," *J. Franklin Inst.*, vol. 349, no. 2, pp. 510–530, Mar. 2012.
[24] D. Efimov, L. Fridman, T. Raïssi, A. Zolghadri, and R. Seydou, "Interval estimation for LPV systems applying high order sliding mode techniques," *Automatica*, vol. 48, no. 9, pp. 2365–2371, 2012.
[25] P. Apkarian, P. Gahinet, and G. Becker, "Self-scheduled H_∞ control of linear parameter-varying systems: A design example," *Automatica*, vol. 31, no. 9, pp. 1251–1261, Sep. 1995.
[26] P. Apkarian and P. Gahinet, "A convex characterization of gain-scheduled H_∞ controllers," *IEEE Trans. Autom. Control*, vol. 40, no. 5, pp. 853–864, May 1995.
[27] Y. M. Jia, *Robust H_∞ Control (in Chinese)*. Beijing, China: Science Press, 2007.
[28] E. Prempain and I. Postlethwaite, "Brief paper: L_2 and H_2 performance analysis and gain-scheduling synthesis for parameter-dependent systems," *Automatica*, vol. 44, no. 8, pp. 2081–2089, Aug. 2008.
[29] T. M. Seigler, "Dynamics and Control of Morphing Aircraft," Ph.D disertation, Virginia Polytech. Inst. State Univ., Blacksburg, VA, USA, 2005.
[30] Public Domain Aeronautical Software, "The USAF stability and control datcom, volume I, users manual," McDonnell Douglas Astronaut. Company, St. Louis, MO, USA, Tech. Rep. AFFDL-TR-79-3032, 1999.
[31] B. Sun, L. Yang, and J. Zhang, "Robust LPV control design based on HOSVD," *J. Beijing Univ. Aeronaut. Astronaut.*, vol. 42, pp. 1536–1542, Jun. 2016.

[32] Y. J. Huang, T. C. Kuo, and H. K. Way, "Robust vertical takeoff and landing aircraft control via integral sliding mode," *IEE Proc.-Control Theory Appl.*, vol. 150, no. 4, pp. 383–388, Jul. 2003.
[33] N. Wen, Z. H. Liu, L. Li, R. Zhou, and L. P. Zhu, "H_∞ control for morphing aircraft via non-affine parameter dependent LPV model (in Chinese)," *J. Beijing Univ. Aeronaut. Astronaut.*, vol. 43, no. 10, pp. 2073–2080, 2017.
[34] J. Lian and J. Zhao, "Robust H-$_\infty$ integral sliding mode control for a class of uncertain switched nonlinear systems," *J. Control Theory Appl.*, vol. 8, no. 4, pp. 521–526, Nov. 2010.

QIAN WU received the bachelor's degree in automation science from the School of Information Science and Technology, Dalian Maritime University, Liaoning, China, in 2017. She is currently pursuing the master's degree with the School of Automation Science and Electrical Engineering, Beihang University, Beijing, China. Her current research interests include advanced aircraft control and high-precision servo system control.

ZHENGHUA LIU received the bachelor's and master's degrees from the School of Mechanical and Electrical Engineering, Nanjing University of Aeronautics and Astronautics, and the Ph.D. degree from the School of Information Science and Technology, Beihang University, Beijing, China.

From 2004 to 2006, he was a Postdoctoral Researcher with the School of Automation Science and Electrical Engineering, Beihang University, where he is currently an Associate Professor. He has presided more than a number of related research projects and engineering projects and published many high-impact papers. His research interests include advanced aircraft control and high-precision servo system control.

FANNING LIU received the bachelor's degree in automation science from Beihang University, Beijing, China, in 2018, where she is currently pursuing the master's degree. Her research interests include flight control and simultaneous localization and mapping (SLAM).

XUEKUN CHEN received the bachelor's degree in automation from the College of Information Science and Technology, Beijing University of Chemical Technology, Beijing, China, in 2017. He is currently pursuing the master's degree with Beihang University, Beijing, China. His research interests include high-precision servo system control and flight control.